

# Development and operation of the twin radio frequency single electron transistor for cross-correlated charge detection

T. M. Buehler, D. J. Reilly, R. P. Starrett, N. A. Court, A. R. Hamilton, A. S. Dzurak and R. G. Clark

*Centre for Quantum Computer Technology, Schools of Physics and Electrical Engineering & Telecommunications,  
University of New South Wales, Sydney 2052, Australia*

Ultra-sensitive detectors and readout devices based on the radio frequency single electron transistor (rf-SET) combine near quantum-limited sensitivity with fast operation. Here we describe a twin rf-SET detector that uses two superconducting rf-SETs to perform fast, real-time cross-correlated measurements in order to distinguish sub-electron signals from charge noise on microsecond time-scales. The twin rf-SET makes use of two tuned resonance circuits to simultaneously and independently address both rf-SETs using wavelength division multiplexing (WDM) and a single cryogenic amplifier. We focus on the operation of the twin rf-SET as a charge detector and evaluate the cross-talk between the two resonance circuits. Real time suppression of charge noise is demonstrated by cross correlating the signals from the two rf-SETs. For the case of simultaneous operation, the rf-SETs had charge sensitivities of  $\delta q_{SET1} = 7.5\mu e/\sqrt{Hz}$  and  $\delta q_{SET2} = 4.4\mu e/\sqrt{Hz}$ .

## I. INTRODUCTION

The radio frequency single electron transistor (rf-SET) is a nano-scale device capable of detecting fractions of an electron charge on sub-microsecond time-scales [1]. In addition to being an exquisite electrometer [2], the rf-SET may also find application as a single photon [3, 4] and particle detector [5], micro-mechanical displacement sensor [6], ultra-high impedance voltage amplifier [7, 8, 9] and ultimately as a fast single-shot read out device in solid-state quantum computers [10]. At present the sensitivity of rf-SETs is primarily limited by the post-amplifier, which is typically a GaAs high-electron mobility transistor (HEMT) operating at  $T \sim 4K$ . In the near future, this limitation is likely to be overcome via the use of rf amplifiers based on a micro-strip dc superconducting quantum interference device (SQUID) which have demonstrated noise temperatures near 100mK at frequencies suitable for rf-SET operation [11]. At low frequencies (below 100kHz), rf-SETs suffer from  $1/f$ -type charge noise associated with the motion of charge in the SET dielectric tunnel barriers and substrate. In particular telegraph noise, that results from charge fluctuators that are strongly coupled to the SET, poses a challenge to the widespread use of rf-SETs as both detectors and readout devices.

In an effort to address the issue of telegraph noise we have utilized two superconducting rf-SETs to form a cross-correlation charge detector, termed a *twin* rf-SET. The cross-correlation technique is advantageous in suppressing charge noise originating from fluctuating traps in the surrounding material system and constitutes a means of discriminating read out signals from spurious charge fluctuations on micro-second time-scales [12]. Independent control of the source-drain bias across each superconducting SET permits both devices to simultaneously operate at the point of maximum sensitivity and measurement efficiency [13]. By making use of wavelength

division multiplexing (WDM) the twin rf-SET provides two (or more) outputs for cross-correlation measurements using only a single cryogenic following amplifier and a single transmission line. Such multiplexed arrangements are highly desirable in instances where arrays of rf-SETs are used as detectors [7].

The article is organized as follows: in Sec. II we briefly review the rf-SET. Sec. III introduces the twin rf-SET and the multiplexing technique. We also discuss our demodulation method that makes use of a mixer-based detection scheme. In Sec. IV we discuss the operation of the resonant circuits and focus on the degree of cross-talk between the circuits and the issues that affect independent operation of the SETs. Additionally we present electromagnetic (EM) simulation results of our circuit and show good agreement with our data. Sec. V presents frequency and time domain data for the case of simultaneous operation. We demonstrate charge sensitivities of  $\delta q_{SET1} = 7.5\mu e/\sqrt{Hz}$  and  $\delta q_{SET2} = 4.4\mu e/\sqrt{Hz}$  and show how the technique of cross-correlation can be used to suppress spurious charge noise on microsecond time-scales.

## II. RF-SET

Normal state SET charge detectors are based on the Coulomb blockade [14] of electrons tunneling across two low capacitance junctions  $J_{1,2}$  ( $C_1, R_1$  and  $C_2, R_2$ ). An ‘island’ with a characteristic charging energy  $E_C = e^2/2C_\Sigma$ , where  $C_\Sigma$  is the capacitive coupling to the environment, is formed between the tunnel junctions. The sequential electron tunneling current across the island can be controlled by the voltage on a gate which is capacitively coupled to the island. Coulomb blockade is effective for temperatures  $T < E_C/k_B$  and for tunneling resistances  $R_{1,2}$  of order of the resistance quantum  $h/e^2 \sim 26k\Omega$ . These restrictions generally limit the op-

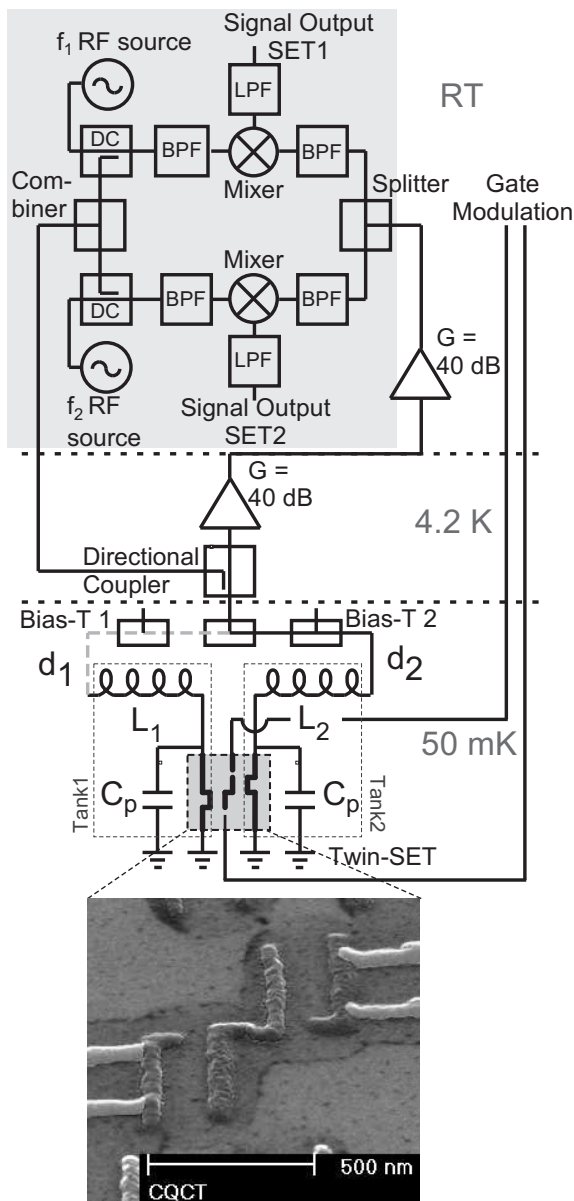


FIG. 1: Schematic of the twin rf-SET setup. Signals are coupled to the tank circuits by using a directional coupler and are then directed to the corresponding SET by the tuned impedance transformers. The reflected signal feeds cryogenic (gain = 40dB) and room temperature (gain = 40dB) amplifiers. Two bias-tees allow independent dc-biasing of each SET. **Shaded region:** Schematic of the rf carrier generation and signal demodulation. The incident carrier wave is produced by combining the output of two independent rf signal generators. **The bottom section** shows a SEM image of a twin-SET device. The tunnel barriers required for Coulomb blockade are formed after the first evaporation step by in-situ oxidation of the aluminum surface. For SET2 (right) the overlaps of source and drain leads (second evaporation) with the SET island (first evaporation) can be seen

vspace-0.5cm

eration of SETs to cryogenic temperatures. Traditionally,

the bandwidth of SETs has been limited to a few kHz by the large  $RC$  time constant associated with the SET output resistance and the capacitance of the wiring from the SET to the room temperature amplifiers. In contrast to the conventional SET, the rf-SET [1] makes use of a  $LC$  impedance transformer to match the impedance of the SET to the characteristic impedance of a transmission line. In this regime, either the reflected [1] or transmitted [15] power of an incident rf carrier wave is a function of the SET resistance. Mapping the device resistance to changes in the reflected or transmitted power thereby allows fast charge detection. In the case of reflection measurements, the incident rf carrier is coupled to the  $LCR$  matching network via a directional coupler and the reflected power is coupled to a low noise cryogenic HEMT amplifier. The  $LCR$  circuit is described by the loaded quality factor  $Q = (Z_{LC}/R_{SET} + Z_0/Z_{LC})^{-1}$ , where  $Z_0$  is the characteristic impedance of the transmission line and  $R_{SET}$  is the differential resistance of the SET and  $Z_{LC} = \sqrt{L/C}$ . The (loaded)  $Q$  factor is inversely proportional to the bandwidth of the impedance matching network.

SETs fabricated from metals that exhibit superconductivity at these temperatures generally also display rich current - voltage characteristics in association with the interplay between charging effects and Cooper pair transport across junctions  $J_1$  and  $J_2$ . Notably, in the vicinity of the threshold voltage for current transport (defined by the superconducting gap and the charging energy), resonant tunneling processes can be observed which are governed by the dynamics of coherent Cooper pair and incoherent quasi-particle transport [16]. Superconducting SETs biased to a Josephson quasi-particle resonance (JQP) have recently been explored in conjunction with reading-out a quantum computer and shown to approach quantum limits for measurement efficiency [13].

### III. TWIN RF-SET SETUP

The technique of wavelength division multiplexing has long been applied in communications engineering as a means of utilizing channel resources efficiently. In line with earlier work on SQUIDs [17], recent work by Stevenson *et al.*, [7] has explored the possibility of using multiplexed rf-SETs to amplify signals from high impedance photon detectors for application in astronomy. Here we extend these results and note that for our case where the SETs are independently biased using bias-tees, a lumped-element circuit analysis is generally inadequate in describing our data. Consequently we present circuit simulation results that account for the length of transmission lines used in our setup [18].

Turning now to the specifics of our setup, we achieve multiplexing of signals from the two rf-SETs via two tuned  $LC$  impedance transformers (Figure 1). Each tank circuit can be approximated by a parasitic capacitance  $C$  to ground and a chip inductor with inductance  $L_{1,2}$ .

The circuits are tuned by choosing appropriate inductances to transform the impedance of the SET (typically 40 - 100k $\Omega$ ) downward towards a characteristic impedance of 50 $\Omega$  at the respective resonant frequency  $\omega_{1,2} = 1/\sqrt{CL_{1,2}}$ . Figure 1 shows a schematic of our cryogenic setup, including two separate bias-tees for independent dc-biasing of each SET. In this setup the length of coaxial transmission line between the ‘T’ section and the SETs (see Figure 1,  $d_1$  dashed line and  $d_2$  solid line) is a critical parameter determining the crosstalk between the SET tank circuits. The ‘T’ arrangement can be considered a single shunt ‘stub’, where the length of the stub and transmission line between the load and the stub position tune the admittance seen looking into the line [19]. In the present experimental arrangement we place our cryogenic HEMT amplifier at the  $T = 4\text{K}$  stage of our dilution refrigerator to avoid the use of cryogenic feed-throughs and to reduce losses between the SET and the amplifier. The twin rf-SET data presented here was taken using tank circuits with resonance frequencies  $f_1 \sim 335\text{MHz}$  and  $f_2 \sim 360\text{MHz}$ , using inductances of 780nH and 660nH, with a total parasitic capacitance estimated to be  $\sim 0.3\text{pF}$  for each SET. The choice of frequencies corresponds to the bandwidth where our cryogenic rf-amplifier [20] maintains optimum noise performance and in addition, where chip inductors are readily available. Variations in the parasitic capacitance  $C$  (and resonance frequency  $\omega$ ) for different samples can be attributed to changes in the length of bond-wires from the inductors to the sample contact pads, changing  $C$  by tens of  $fF$ .

The incident carrier wave is produced by combining the output of two independent rf signal generators (Figure 1). Each generator output is fed to a directional coupler in order to tap off power (-16dB) for the SETs. The remaining signal (-0.11dB) is directed to the mixers as a reference signal. A subsequent splitter/combiner is used to feed the two frequencies to one semi-rigid coaxial waveguide into the cryostat. After the signal enters the cryostat the rf power is coupled to the tank circuits using another directional coupler. The signals  $f_{1,2}$  are directed to SET $_{1,2}$  by the tuned impedance transformers, tank $_{1,2}$ . The reflected signal is then coupled to the cryogenic amplifier (40dB gain) and a room temperature amplifier (40dB gain). A power splitter feeds the reflected rf signal to two mixers for demodulation. High roll-off, narrow bandpass filters [21] are used before both the local oscillator (LO) and RF mixer inputs to suppress intermodulation distortion [19] and higher order components. Active phase-shifters are used to ensure constructive interference of RF and LO inputs at the mixer. Finally, the intermediate frequency (IF) mixer product is low-pass filtered before being output into either a multichannel oscilloscope or spectrum analyzer for time and frequency domain measurements respectively. To further improve signal quality we also use various attenuators and filters at room and cryogenic temperatures.

The lower part of Figure 1 shows a SEM image of an

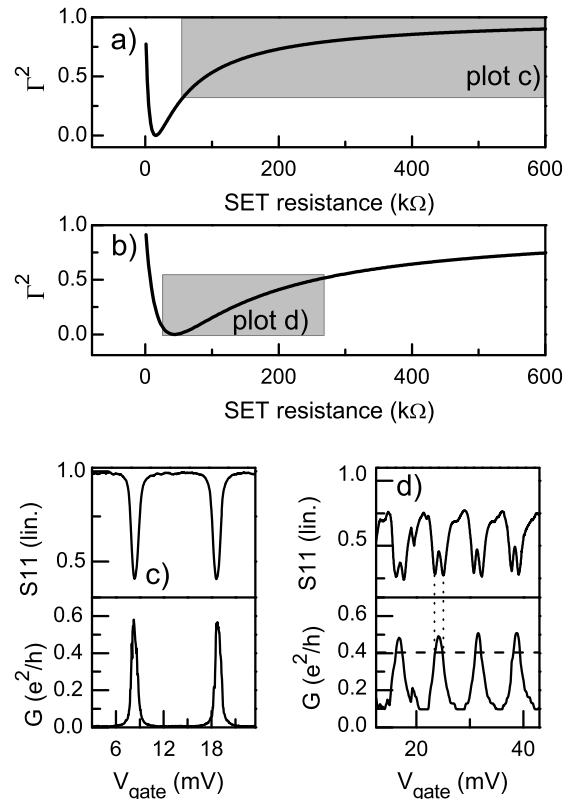


FIG. 2: **a)** and **b)** Lumped element calculations of the power reflection coefficient as a function of the SET resistance for impedance transformers designed to match 17k $\Omega$  to  $Z_0 = 50\Omega$  for a) and 50k $\Omega$  to  $Z_0$  for b). The shaded regions correspond to the matching regimes shown in c) and d). **c)** Reflected rf power (top,  $S_{11}$ ) and dc conductance (bottom) in the superconducting state. The SET resistance remains above 17k $\Omega$  (note the different scale on the y-axis) throughout and the impedance transformer operates in the under-matched regime. **d)** Reflected rf power (top,  $S_{11}$ ) and dc conductance (bottom) with the SET biased to a region where the resistance at the top of a peak is less than 50k $\Omega$ . The non-monotonic dependence on gate bias arises as the operating point moves from under to over matched.

$Al/Al_2O_3$  twin-SET device used in these experiments. The device was fabricated using electron beam lithography and the standard shadow mask evaporation technique [22]. The tunnel junctions are formed where the leads (horizontal) overlap with the ‘islands’ (vertical). In this arrangement the SETs are  $\sim 500\text{nm}$  apart and control gates used in these experiments couple to both SETs inducing charges of similar magnitude on both devices. In addition there is a central double-dot structure, developed for read out simulations but not relevant to the measurements described here [12].

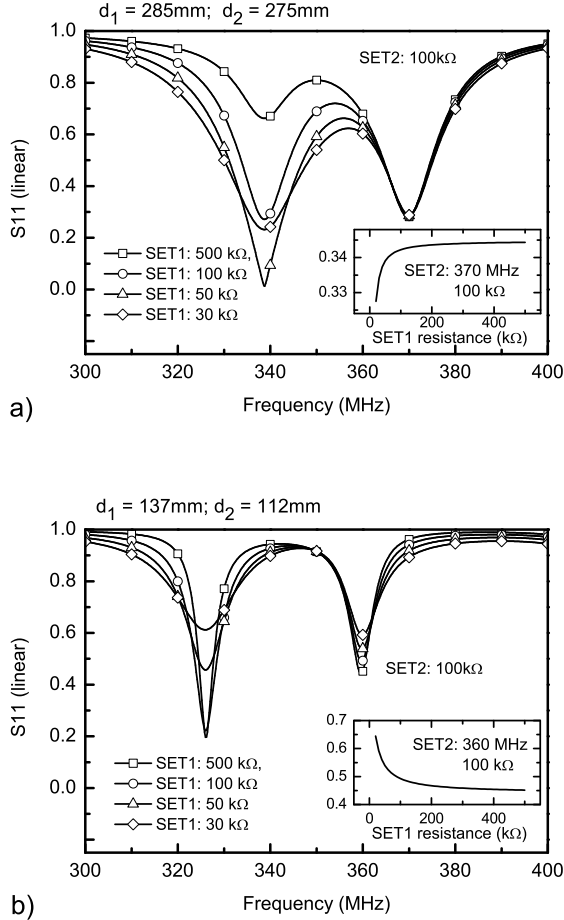


FIG. 3: Simulation results [18] showing the effect of shunt stub tuning. **a)** Shows the ideal case where cross-talk is kept to a minimum ( $d_1 = 285\text{mm}$  and  $d_2 = 275\text{mm}$ ). As indicated by the inset,  $S_{11}$  at  $\omega_2$  is hardly effected by varying the resistance of SET1, only varying slightly in the over-matched case. Contrasting this behavior **b)** shows simulation results for an unoptimized stub network. In this scenario the cross talk between the two tank circuit is near 50% despite the increased  $Q$  factor. For clarity the *linear*  $S_{11}$  is shown.

#### IV. TANK CIRCUIT CHARACTERIZATION

In order to maximize the sensitivity of the rf-SET, the device should be operated in a regime where the amount of reflected power depends most strongly on the SET resistance. Figures 2a and 2b show the calculated power reflection coefficient  $\Gamma^2$  ( $\Gamma = (Z_0 - Z_{LCR})/(Z_0 + Z_{LCR})$ ) in a *single* rf-SET arrangement as a function of the SET resistance for two different matching networks. For Figure 2a the tank circuit  $LC$  values were chosen to transform a  $17\text{k}\Omega$  impedance to  $Z_0$  ( $50\Omega$ ) at resonance and for Figure 2b to transform  $50\text{k}\Omega$  to  $Z_0$ . For perfect matching the power reflection coefficient then approaches zero when the SET resistance is  $17\text{k}\Omega$  for figure 2a and  $50\text{k}\Omega$

for figure 2b. We discuss two modes of operation, the under-matched (or under-coupled) regime, where the device resistance is greater than the matching resistance and the over-matched (or over-coupled) regime where the device resistance is smaller than the matching resistance. Over-matching yields an enhanced depth of modulation in association with the large slope of  $\Gamma^2$  as a function of the SET resistance, but reduces the  $Q$  factor [23].

Figures 2c and 2d show measurement results for a single rf-SET. The reflected rf power (top) is measured together with the dc conductance (bottom) as a function of gate voltage. The data shown in Figure 2c is limited to the under-matched regime, where the resistance of the SET is always greater than  $17\text{k}\Omega$ . The corresponding behavior of the reflection coefficient is indicated in Figure 2a by the darker shaded region. In this regime the reflected power increases monotonically with increasing SET resistance, so that the  $S_{11}$  data shown in Figure 2c is a mirror image of the SET conductance. In contrast, the data shown in Figure 2d was taken with the SET biased to a point where the differential resistance is less than  $50\text{k}\Omega$  at the top of a Coulomb blockade peak. Moving from the blocked state to a point where the differential resistance is less than  $50\text{k}\Omega$  results in a non-monotonic response in the reflected rf power as shown in the upper section of Figure 2d. This behavior is due to the impedance transformer operating initially in the under-matched regime and moving to over-matching as the differential resistance moves through  $50\text{k}\Omega$ , as indicated by the dark shaded region in Figure 2b. The non-monotonic behavior of the transfer function in the over-matched regime complicates operation of the device as a charge detector, as seen in the upper panel of Figure 2d. Over-matching also reduces the  $Q$ -factor so that in a multiplexed arrangement the resonances need to be separated further in frequency to minimize cross-talk.

Turning now to simultaneous operation of both SETs we note that if there was no cross-coupling between the two circuits, then the output signal for tank2 should be independent of the resistance of SET1. Clearly cross-talk is a function of the overlap between the two resonance traces defined by their ‘single circuit’  $Q$  factors, so that the resonance frequency of the two circuits should be well separated to minimize cross-talk. In spite of well separated resonances however, additional effects can strongly modify the cross-talk between the two SETs. We now discuss the dominant mode of cross-talk in our setup. In the multiplexed arrangement shown in Figure 1, the branching ‘T’ section behaves as a stub tuning network since at the resonant frequency of SET1, tank2 appears as a load at the end of a length of transmission line in parallel with the transmission feed-line to SET1. The impedance seen looking into the ‘T’ section is [19],  $1/Z_{in} = 1/Z_1 + 1/Z_2$ , where

$$Z_{1,2}(\omega_{1,2}, d_{1,2}) = Z_0 \frac{Z_{\text{tank}1,2} + jZ_0 \tan \beta d_{1,2}}{Z_0 + jZ_{\text{tank}1,2} \tan \beta d_{1,2}} \quad (1)$$



and  $\beta = 2\pi/\lambda_{1,2}$ . For the case where the tank circuits are well separated in frequency, with tank2 close to an open circuit for  $\omega_1$ ,

$$Z_2 = -jZ_0 \cot \beta d_2 \quad (2)$$

so that the impedance  $Z_{1,2}$  at  $\omega_1$  looking into the ‘T’ section is just determined by  $d_1$ ,  $d_2$  and  $Z_{\text{tank}1}$ . In an ideal arrangement  $d_2$  should be of zero length, or adjusted so that the impedance  $Z_2$  appears as an open line. If this condition is achieved the amount of reflected power is solely determined by  $Z_{\text{tank}1}$ . In the case where this is not achieved, the stub geometry and length of the transmission lines between the ‘T’ and the SET tank circuits strongly affect both the impedance matching of the  $LC$  network to the SETs and the degree of cross-talk between the two circuits. Figure 3a and 3b compare the two cases of ‘length matching’ using an EM simulation software package [18]. Optimum length matching is illustrated in Figure 3a where  $S_{11}$  is plotted as a function of frequency for different values of SET1 resistance, including both under-matching ( $\text{SET} > 50\text{k}\Omega$ ) and over-matching ( $\text{SET} < 50\text{k}\Omega$ ). The resistance of SET2 is held constant at  $100\text{k}\Omega$  and inductances  $L_1=780\text{nH}$ ,  $L_2=660\text{nH}$  define the resonances at  $\omega_1=339\text{MHz}$  and  $\omega_2=370\text{MHz}$  for a parasitic capacitance  $C=0.3\text{pF}$ . With transmission line lengths set at  $d_1 = 285\text{mm}$  and  $d_2 = 275\text{mm}$ , near independent operation of the SETs can be achieved. The inset shows the variation in  $S_{11}$  at  $\omega_2$  as a function of SET1 resistance. Only in the over-matched case ( $R_{\text{SET}1} = 30\text{k}\Omega$ ) does the resistance of SET1 weakly affect the reflected power at  $\omega_2$ . Turning to the unoptimized case illustrated in Figure 3b ( $d_1 = 137\text{mm}$  and  $d_2 = 112\text{mm}$ ) we firstly note that the variation in line length has altered the resonant frequencies ( $\omega_{1,2}$ ) and  $Q$ -factors of the circuits in comparison with the results shown in Figure 3a. Additionally the degree of cross-talk is now greatly increased as shown in the inset to Figure 3b. In particular, for the case where SET1 is operated in the over-matched regime, a poorly tuned stub network can create cross-talk signals as large as 50%.

The above discussion, in which the length of transmission line between the ‘T’ section and the SET tank circuits strongly affects both matching and cross-talk, is valid in the regime where line lengths approach or exceed  $\lambda/4$ , which at these frequencies is the order of centimeters. Although the use of micro-strip or strip-line techniques can be used to avoid this issue, we note that the constraint of independent source-drain biasing for each SET requires the incorporation of a bias-tee in the transmission line in between the ‘T’ junction and SETs. Bias-tees typically contain several inductors of appreciable size and are not easily miniaturized with low insertion loss and good standing wave ratios. Of further interest, a stub network (or double-stub) could be used as an impedance matching technique without the requirement of chip inductors commonly used for impedance matching in the rf-SET. With the addition of a varactor diode terminating the stub, the value of the reactance provided by the stub

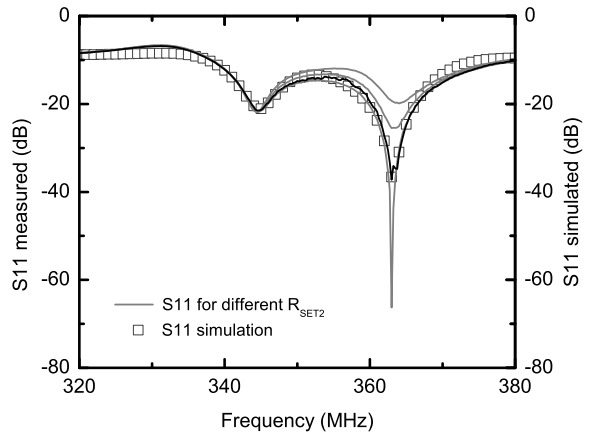


FIG. 4: Comparison between simulation results and experimental data. For the experimental data  $L_1=780\text{nH}$ ,  $L_2=660\text{nH}$ ,  $C=0.3\text{pF}$ ,  $\omega_1=345\text{MHz}$ ,  $\omega_2=364\text{MHz}$ ,  $R_{\text{SET}1} > 10\text{M}\Omega$  and  $R_{\text{SET}2}$  varies from  $>10\text{M}\Omega$  (top) to  $\sim 43\text{k}\Omega$  (bottom). We adjust the lengths of the stub network and the length of the bond wires linking the chip to the circuit board as fitting parameters. Small deviations between the simulation results and experiment are most likely due to the input impedance of the cryogenic amplifier, which deviates from  $50\Omega$  across the frequency span.

can be varied with an applied voltage. Such a technique would have several advantages over the present lumped-element matching technique, including *in-situ* control of the matching and  $Q$ -factor.

We now compare our simulation results with experimental data. Figure 4 shows  $S_{11}$  data taken with a network analyzer for varying SET2 resistances,  $\sim 43\text{k}\Omega$  (minimum  $S_{11}$  at  $364\text{MHz}$ ) to  $>10\text{M}\Omega$  (maximum  $S_{11}$  at  $364\text{MHz}$ ). The resistance of SET1 is kept constant throughout ( $R_{\text{SET}1} \sim 10\text{M}\Omega$ , biased in the superconducting gap). Using the microwave simulation package we are able to produce  $S_{11}$  traces that approximate our experimental results. As fitting parameters we adjust the length of transmission lines  $d_1$  and  $d_2$  in the simulation, since these are difficult to measure experimentally at mK temperatures. The values used here ( $d_1=313\text{mm}$ ,  $d_2=304\text{mm}$ ) in the simulation results however, are in agreement with what we expect for our setup. In this arrangement the cross-talk between the tank circuits is limited to  $< 5\%$ , which is close to its minimum value for this frequency separation and the SET resistance range. For the simulation results we also tune the length of the bond wire between our circuit board and chip, and the input impedance of our cryogenic microwave amplifier [20]. The amplifier impedance deviates from the ideal case of  $50\Omega$  since it contains an input network to achieve noise matching to the first-stage transistor. Simultaneous noise and impedance matching are generally not achieved, with the result being a reduction in signal level at the output in order to maximize the signal-to-noise ratio [24]. Fur-

ther weak deviations between our experimental data and the simulation results are most likely due to an inaccurate frequency dependence of the simulated amplifier input impedance and the variation in parameters characterizing our circuit elements with temperature.

## V. SENSITIVITY AND CHARGE NOISE REJECTION

We now present measurement results for simultaneous operation of two rf-SETs, beginning with the charge sensitivities. The data shown in Figure 5 was taken with the SETs in the superconducting regime. Operating the twin rf-SET in the superconducting mode maximizes the device sensitivity, since the transconductance and small signal differential conductance are maximized. Figure 5a shows frequency domain data for both rf-SETs in response to a 2.5 MHz sine wave signal applied to a gate with a rms amplitude of  $\sim 0.1e$  on each SET island. Clear amplitude modulation (AM) of both rf carriers is observed. The sensitivity of the rf-SET can now be determined by measuring the signal to noise ratio (SNR) of either sideband for a rms induced charge signal  $q_{rms}$  on the SET island. The spectral density of the noise is calculated as follows [25]:

$$\delta q = \frac{q_{rms}}{\sqrt{B} \times 10^{SNR/20}} (e/\sqrt{Hz}) \quad (3)$$

where  $B$  is the chosen resolution bandwidth of the spectrum analyzer. For the twin rf-SET device studied here, we measure an optimum sensitivity of  $\delta q = 7.5\mu e/\sqrt{Hz}$  and  $\delta q = 4.4\mu e/\sqrt{Hz}$  for SET1 and SET2 with resonances at 335MHz and 360MHz respectively. The sensitivities were measured for  $q = 0.005e$  signals at 1.3 MHz in the dc+rf (superconducting) mode [25]. The frequency dependence of the noise floor shown in Figure 5a is primarily linked to the frequency dependence of the noise temperature of the cryogenic amplifier, which reaches a minimum of  $T_N \sim 1.5K$  at  $\omega \sim 350MHz$ . Additional (weak) contributions include shot noise associated with the SET current, phase noise of our rf sources,  $1/f$  noise in the SETs and electronics and the frequency dependent noise of the room temperature amplifiers and mixers.

Focusing on the response of the SETs in the time domain, we now demonstrate the suppression of charge noise via cross-correlated measurements. Figure 5b shows the response of both SETs (measured simultaneously) when a 1 kHz square wave is applied to a nearby gate via a 40 dB attenuator. This signal induces charges of  $\sim 0.1e$  and  $\sim 0.05e$  on the islands of SET1 and SET2 respectively. Although the output of the two SETs faithfully follow the gate signal, additional unwanted charge noise is also picked up by SET2 (e.g. in the 0.7 - 1 ms time interval). The observed random telegraph signals (RTSs) are probably associated with charge noise arising from two-level charge traps in the SET oxide tunnel

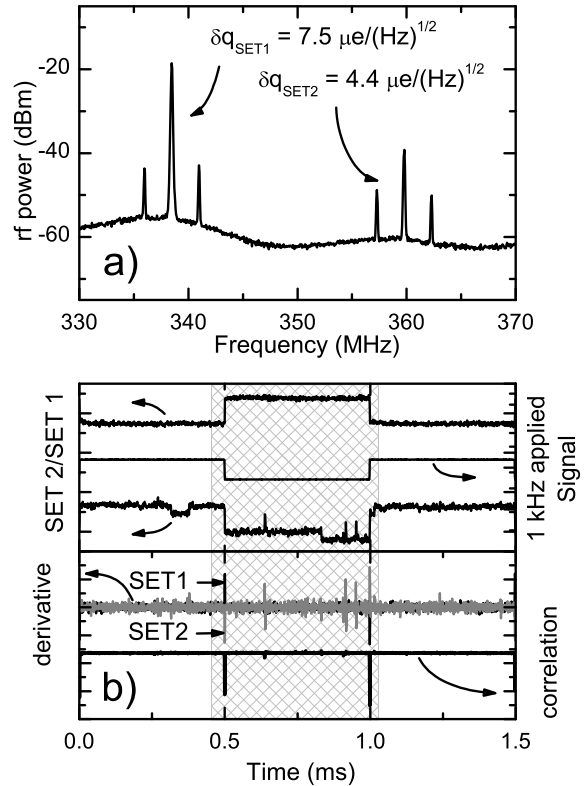


FIG. 5: **a)** Typical amplitude modulation (AM) signal associated with both the SETs responding to a  $\sim 0.1e$ , 2.5MHz gate signal. Charge sensitivities for each device are stated for the case of simultaneous operation (different measurement). **b)** time domain data taken simultaneously with both SETs. Both devices respond independently to a 1KHz square wave signal applied to a nearby gate. Spurious charge noise is superimposed on the output of SET2 (shown in the hashed region). By cross-correlating the signals from both SETs (multiplying the derivatives) we are able to suppress spurious charge noise events in real time.

barrier or substrate. Using a multi-channel digital oscilloscope, we are able to multiply the time derivative signals from SET1 and SET2 in *real-time*. The result is shown in the lower portion of Figure 5b and constitutes a real-time cross-correlation of the SET signals. Close inspection of the correlation trace shows that this technique produces sharp spikes when there is a true signal that affects both SETs (such as the rising or falling edges of the square wave applied to the gate) and a clear suppression of the random charge noise by up to 95% of the peak height correlation. This ability to reject events associated with charge noise is likely to be important for the application of SETs as detectors and in the readout of solid state quantum computers.

## VI. CONCLUSION

In conclusion we have described the development of a twin rf-SET device that makes use of two tuned impedance transformers to perform wavelength division multiplexing (WDM) using a single cryogenic following amplifier. In conjunction with a mixer-based demodulation technique, we have explored the issues affecting cross-talk and sensitivity. The twin rf-SET has been shown to perform real time cross-correlation of SET signals. Such a correlation technique suppresses charge noise and enables true signals associated with readout to be distinguished from spurious artifacts on time-scales required for solid state quantum computation. Future

work will investigate the use of the twin rf-SET for charge motion detection on microsecond time-scales, and its application to readout of both semiconducting and superconducting charge qubits.

We thank D. Barber for technical support and S. Kenyon, K. Lehnert and R. Schoelkopf for fruitful discussions and insights. This work was supported by the Australian Research Council, the Australian Government and by the US National Security Agency (NSA), Advanced Research and Development Activity (ARDA) and the Army Research Office (ARO) under contract number DAAD19-01-1-0653. DJR acknowledges a Hewlett-Packard Fellowship.

---

[\*] email: tbuehler@phys.unsw.edu.au

- [1] R. J. Schoelkopf, P. Wahlgren, A. A. Kozhevnikov, P. Delsing, and D. E. Prober, *Science* **280**, 1238 (1998).
- [2] M. H. Devoret and R. J. Schoelkopf, *Nature (London)* **406**, 1039 (2000).
- [3] S. Komiyama, O. Astafiev, V. Antonov, T. Kutsuwa, and H. Hirai, *Nature (London)* **403**, 405 (2000).
- [4] R. J. Schoelkopf, S. H. Moseley, C. M. Stahle, P. Wahlgren, and P. Delsing, *IEEE Trans. Appl. Supercond.* **9**, 2935 (1999).
- [5] V. Bouchiat, G. Chardin, M. H. Devoret, and D. Esteve, *Hyperfine Interact.* **109**, 345 (1997).
- [6] M. P. Blencowe and M. N. Wybourne, *Appl. Phys. Lett.* **77**, 3845 (2000).
- [7] T. R. Stevenson, F. A. Pellerano, C. M. Stahle, K. Aida, and R. J. Schoelkopf, *Appl. Phys. Lett.* **80**, 3012 (2002).
- [8] K. Segall, K. W. Lehnert, T. R. Stevenson, R. J. Schoelkopf, P. Wahlgren, A. Aassime, and P. Delsing, *Appl. Phys. Lett.* **81**, 4859 (2002).
- [9] T. R. Stevenson, A. Aassime, P. Delsing, R. Schoelkopf, K. Segall, and C. M. Stahle, *IEEE Trans. Appl. Supercond.* **11**, 692 (2001).
- [10] A. Aassime, G. Johansson, G. Wendin, R. J. Schoelkopf, and P. Delsing, *Phys. Rev. Lett.* **86**, 3376 (2001).
- [11] R. Bradley, J. Clarke, D. Kinion, L. J. Rosenberg, K. van Bibber, S. Matsuki, M. Muck, and P. Sikivie, *Rev. Mod. Phys.* **75**, 777 (2003).
- [12] T. M. Buehler, D. J. Reilly, R. Brenner, A. R. Hamilton, A. S. Dzurak, and R. G. Clark, *Appl. Phys. Lett.* **82**, 577 (2003).
- [13] A. A. Clerk, S. M. Girvin, A. Nguyen, and A. D. Stone, *Phys. Rev. Lett.* **89**, 176804 (2002).
- [14] H. Grabert and M. H. Devoret, *NATO Adv. Study Inst. Ser., Ser. B* **294** (1992).
- [15] T. Fujisawa and Y. Hirayama, *Appl. Phys. Lett.* **77**, 543 (2000).
- [16] T. Fulton, P. Gammel, D. Bishop, L. Dunkelberger, and G. Dolan, *Phys. Rev. Lett.* **63**, 1307 (1989).
- [17] M. Muck, *IEEE Trans. Magn.* **27**, 2986 (1991).
- [18] *Microwave Office*, Applied Wave Research, Inc. ([www.appwave.com/products/mwoffice/](http://www.appwave.com/products/mwoffice/)).
- [19] D. M. Pozar, *Microwave Engineering* (Wiley) (1998).
- [20] The cryogenic amplifier is manufactured by Berkshire Technologies Inc. and achieves a noise temperature  $T_N < 2\text{K}$  at 20K case temperature. The bandwidth is 310MHz - 410MHz, with a gain of 40dB. ([www.berkshiretech.com](http://www.berkshiretech.com)).
- [21] The narrow bandpass filters were custom built by Reactel ([www.reactel.com](http://www.reactel.com)).
- [22] T. A. Fulton and G. J. Dolan, *Phys. Rev. Lett.* **59**, 109 (1987).
- [23] L. Roschier, P. Hakonen, K. Bladh, P. Delsing, K. W. Lehnert, L. Spietz, and R. J. Schoelkopf, *Journal of Applied Physics.* **95**, 1274 (2004).
- [24] J. B. Hagen, *Radio-Frequency Electronics* (Cambridge University Press) (1996).
- [25] A. Aassime, D. Gunnarsson, K. Bladh, and Delsing, *Appl. Phys. Lett.* **79**, 4031 (2001).